Nonequilibrium chemistry in confined environments: A lattice Brusselator model

D. Bullara,* Y. De Decker, and R. Lefever
Center for Nonlinear Phenomena and Complex Systems (CENOLI), Code Postal 231, Université Libre de Bruxelles, 1050 Brussels, Belgium
(Received 26 February 2013; published 27 June 2013)

In this work, we study the effect of molecular crowding on a typical example of a chemical oscillator: the Brusselator model. We adopt to this end a nonequilibrium thermodynamic description, in which the size of particles is introduced via a lattice gas model. The impenetrability and finite volume of the species are shown to affect both the reaction rates and the diffusion terms in the evolution equations for the concentrations. The corrected scheme shows a more complex dynamical behavior than its ideal counterpart, including bistability and excitability. These results help to shed light on recent experimental and computational studies in biochemistry and surface chemistry, in which it was shown that confined environments may greatly affect chemical dynamics.

DOI: 10.1103/PhysRevE.87.062923 PACS number(s): 82.40.Bj, 05.70.Ln, 82.20.−w, 82.40.Np

I. INTRODUCTION

It is by now well established that in open systems, chemical reactions can give rise to complex spatiotemporal phenomena if they are maintained far away enough from their equilibrium state [1]. One of the most striking examples of such behaviors is the emergence of oscillations of concentrations in time and space. Such chemical oscillations have been observed in many instances including redox reactions, heterogeneous catalytic systems, and biological cells, to cite a few.

From a theoretical point of view, the above-mentioned oscillations are typically modeled using partial differential equations (PDEs) that govern the evolution of each species' concentration c_i in space and time. In the case of an isothermal system at mechanical equilibrium, one for example uses *reaction-diffusion equations* that express the rate of change of local concentrations:

$$\frac{\partial}{\partial t}c_i(\mathbf{r},t) = -\nabla\cdot\Phi_i[\{c_j(\mathbf{r},t)\}] + \sigma_i[\{c_j(\mathbf{r},t)\}]. \qquad (1)$$

The two contributions to this rate are respectively (i) a transport of mass, Φ_i being the total flux of species i, and (ii) a local creation or destruction of particles by chemical reactions, σ_i being the total local production rate. In most situations, the transport is modeled by Fick's law $\Phi_i[\{c_j(\mathbf{r},t)\}] = -D_i\,\nabla c_i(\mathbf{r},t)$, where D_i is a constant diffusion coefficient. The reaction rate can be estimated by decomposing the chemical reactions into a set of elementary steps

$$\sum_{i=1}^{\alpha} a_{i,\rho}\,X_i \rightleftharpoons \sum_{i=1}^{\alpha} \ell_{i,\rho}\,X_i, \qquad (2)$$

where X_i stands for one of the α different species, and $a_{i,\rho}$ ($\ell_{i,\rho}$) is the molecularity of each reactant (product) in the reaction ρ. The rate associated with each of these events is then typically given by the mass action law. The dynamical complexity of models derived in this way originates in the intrinsically nonlinear character of these reaction rates (in terms of concentrations), leading to intricate time-dependent and/or stationary solutions of the above PDEs.

We asses here the validity of such an approach in the case of reactions taking place in spatially constrained systems, which can lead to highly crowded environments. This problem attracted much attention recently, e.g., in the framework of chemical reactions on surfaces [2,3] or in intracellular environments [4–6]. It was shown that the above equations are then unable to reproduce the dynamical behavior observed through microscopic simulations. Comparison between these two levels of descriptions has led to the following observations: Steady states seem to be displaced, to disappear, or to appear; the stability of these states can change; dynamical phenomena predicted by the above laws are not observed or are qualitatively different [7,8]. For example, several models which are known to produce oscillations in a reaction-diffusion approach were simulated on low-dimensional regular lattices. A lattice Lotka-Volterra model has been studied, for which it was observed that oscillations disappear in one dimension and that the frequency of oscillations depends on the lattice coordination in higher-dimensional systems [9]. Shabunin *et al.* simulated and analyzed a kinetic model giving rise to a limit cycle and showed that sustained oscillations could be lost on two-dimensional lattices [10]. Zhdanov also reported a disappearance of oscillation, in the case of a lattice-compatible version of the Brusselator model [11]. More recently, the same model has also been used to develop multiscale techniques on two-dimensional lattices: It was once more observed that temporal oscillations are lost (for low species mobilities) [12]. None of these works on the Brusselator model, however, was supported by an analysis of the underlying dynamical system.

The usual explanation for the observed discrepancies is that, because of the spatial constraints, fluctuation-induced correlations between the particles can build up and dictate the system's dynamics. Since they neglect fluctuations, reaction-diffusion equations should then be replaced by a stochastic level of description. We believe, however, that, on too many occasions, these conclusions have been drawn by overlooking an important question: Are not the spatial restrictions supposed to affect the reaction-diffusion equations themselves? In this work we propose to answer this question using nonequilibrium thermodynamics and to analyze how such changes affect the dynamics of oscillatory reactions. More specifically, we use this approach to investigate the dynamical properties of a *lattice-compatible* version of the Brusselator. This choice is mainly motivated (i) by the simplicity (and the thermodynamically clear picture) of the original Brusselator model that has already been studied in great detail, and (ii) by the fact that

*dbullara@ulb.ac.be

its implementation on a regular lattice represents a simple and natural way of introducing restricted geometries.

In Sec. II, we present the model and extract the corresponding reaction-diffusion equations. We show that spatial restrictions play a major role, by modifying both the reaction and transport terms. We next show in Sec. III that the lattice Brusselator reveals especially rich structure, and can present additional bifurcations as compared to the classical Brusselator even in the limit of perfectly stirred systems. Section IV is devoted to an analysis of the spatially distributed case: We demonstrate how the constrained medium affects the emergence of reaction-diffusion instabilities in the system. We finally discuss the limits of applicability of this approach and possible extensions (in Sec. V).

II. DERIVATION OF THE REACTION-DIFFUSION EQUATIONS

The model we investigate is a version of the Brusselator model [13]

$$A \to X, \tag{3}$$

$$B + X \to Y + D, \tag{4}$$

$$2X + Y \to 3X, \tag{5}$$

$$X \to E, \tag{6}$$

where the intermediate species X and Y are kept in a geometrically restricted medium. This environment is seen as a continuum of mesoscopic, pointlike boxes of constant volume ΔV centered at positions $\mathbf{r}$. To model the spatial restriction, we endow each of these boxes with a regular discrete lattice structure, having a large (and identical) number N_t of nodes. Each node can either be occupied by one X particle or one Y particle or stay free (we denote such empty sites with the symbol $*$). This feature is introduced to account for the impenetrability of the different species, eventually leading to crowding. As a consequence, the following conservation law holds between the number of lattice sites occupied by the different species in each box:

$$N_X(\mathbf{r},t) + N_Y(\mathbf{r},t) + N_*(\mathbf{r},t) = N_t = \text{const}. \tag{7}$$

The coarse graining introduced by this description allows one to define local concentrations $c_i(\mathbf{r},t) = N_i(\mathbf{r},t)/\Delta V$. Since one of the three concentrations is fixed by the balance $c_X + c_Y + c_* = c_t = \text{const}$, it suffices to consider the evolution equations for the two remaining variables:

$$\frac{\partial}{\partial t} c_X(\mathbf{r},t) = -\nabla \cdot \Phi_X[\{c_j(\mathbf{r},t)\}] + \sigma_X[\{c_j(\mathbf{r},t)\}], \tag{8}$$

$$\frac{\partial}{\partial t} c_Y(\mathbf{r},t) = -\nabla \cdot \Phi_Y[\{c_j(\mathbf{r},t)\}] + \sigma_Y[\{c_j(\mathbf{r},t)\}]. \tag{9}$$

At this level, these equations still need to be closed with relations connecting the fluxes and reaction rates directly to c_X and c_Y.

Before we move on to the derivation of the evolution laws, some important comments should be made on the compatibility of the Brusselator model with the imposed spatial constraints. The reaction scheme (3)–(6) is not compatible with Eq. (7), which imposes at each elementary step the balance $\nu_X + \nu_Y + \nu_* = 0$, a condition that the first and last steps do not satisfy. In other words, one needs to modify the Brusselator model to make it *lattice compatible*. This leads to the Lattice Brusselator model, which reads

$$A + * \to X, \tag{10}$$

$$B + X \to Y + D, \tag{11}$$

$$2X + Y \to 3X, \tag{12}$$

$$X \to E + *. \tag{13}$$

This scheme can be interpreted as a chemical reaction occurring between two different phases: a confined medium where only X and Y are present (along with the empty sites $*$), and an external reservoir, in which geometrical constraints do not apply, and where the other reactants and products (namely, A, B, D, and E) are stored. In this framework the first step of the lattice Brusselator corresponds to the passage of one molecule of A from the reservoir into the confined environment, where it becomes X; this process "consumes" one empty lattice site. Similarly, when X leaves the restricted environment to give E, it also frees one empty site in the process.

A. Reaction rates

The above reaction and transport terms can be directly derived from the chemical potential, by adopting the local equilibrium assumption [14]. Since we consider isothermal systems with constant ΔV, the local chemical potentials are given by

$$\mu_i(\mathbf{r},t) = \mu_i^0(T) + k_B T \ln c_i(\mathbf{r},t), \tag{14}$$

where μ_i^0 is the standard chemical potential (see, for example, [15]). Despite the geometrical constraint imposed by the lattice, the chemical potentials take the same form as in ideal mixtures. The conservation law (7) however implies that these potentials are not independent of each other: This will play a central role in the rest of the derivation.

The reaction rate of each reaction ρ can be related to its affinity $\mathscr{A}_\rho(\mathbf{r},t) = -\sum_{i=1}^{\alpha} \nu_{i,\rho}\, \mu_i(\mathbf{r},t)$ via the general relation [16]

$$v_\rho = \frac{1}{\tau_\rho} e^{(\sum_i^\alpha \alpha_{i,\rho}\mu_i)/k_B T}[1 - e^{-\mathscr{A}_\rho/k_B T}] \equiv \frac{1}{\tau_\rho} e^{(\sum_i^\alpha \alpha_{i,\rho}\mu_i)/k_B T},$$

since we consider irreversible reactions, for which $\mathscr{A}_\rho \to \infty$. The reaction's characteristic time τ_ρ cannot be estimated from nonequilibrium thermodynamics, but requires some additional kinetic information. We will consider the simple case for which these time scales are not affected by the composition of the system (as in, for example, the collision model of reactions). One can then write the local reaction rates for each species:

$$\sigma_X = k_1 a_A\, c_*(\mathbf{r},t) - [k_2 a_B + k_4] c_X(\mathbf{r},t) + k_3 c_X^2(\mathbf{r},t) c_Y(\mathbf{r},t), \tag{15}$$

$$\sigma_Y = k_2 a_B c_X(\mathbf{r},t) - k_3 c_X^2(\mathbf{r},t) c_Y(\mathbf{r},t). \tag{16}$$

The kinetic constants k_j are a combination of the intrinsic time scales and the standard chemical potentials, which are supposed to be independent of concentrations, space, and time: $k_1 = \frac{1}{\tau_1} e^{(\mu_A^0 + \mu_*^0)/k_B T}$, $k_2 = \frac{1}{\tau_2} e^{(\mu_B^0 + \mu_X^0)/k_B T}$,

$k_3 = \frac{1}{\tau_3}\, e^{(2\mu_X^0+\mu_Y^0)/k_BT}$, $k_4 = \frac{1}{\tau_4}\, e^{\mu_X^0/k_BT}$. These equations display the usual mass-action laws, where a_i represents the activity of the particles in the reservoirs, which are assumed to be maintained constant. The nonideality, however, reflects itself through the conservation law (7) acting upon the concentrations. This effect will be discussed in more detail in Sec. III.

B. Mass transport

Some care has to be taken when estimating the transport terms appearing in the evolution equations (8) and (9). The conservation law (7) implies that

$$\nabla \cdot [\Phi_X + \Phi_Y + \Phi_*] = 0, \tag{17}$$

which can be interpreted as an *incompressibility condition* for the total molar density c_t. Since we also assumed no net flow of particles at the boundaries and no external force field, the dynamics of the system reduces to a purely reactive-diffusive problem in the sense that there is locally no net flux of particles: $\Phi_X + \Phi_Y + \Phi_* = \mathbf{0}$.

It can be shown, starting from the classical general expression for the entropy production (see the Appendix), that the generalized forces associated with each molar flux Φ_i are here given by $T^{-1}\,\nabla_{T,p}[\mu_j(\mathbf{r},t) - \mu_*(\mathbf{r},t)]$. By using Curie-Prigogine's symmetry principle and Onsager's reciprocity relations, one can therefore linearly expand the two remaining molar diffusive fluxes as

$$\Phi_X = -L_{XX}\frac{\nabla_{T,p}[\mu_X(\mathbf{r},t) - \mu_*(\mathbf{r},t)]}{T} - L_{XY}\frac{\nabla_{T,p}[\mu_Y(\mathbf{r},t) - \mu_*(\mathbf{r},t)]}{T}, \tag{18}$$

$$\Phi_Y = -L_{XY}\frac{\nabla_{T,p}[\mu_X(\mathbf{r},t) - \mu_*(\mathbf{r},t)]}{T} - L_{YY}\frac{\nabla_{T,p}[\mu_Y(\mathbf{r},t) - \mu_*(\mathbf{r},t)]}{T}. \tag{19}$$

We here assume that the cross-coupling coefficient L_{XY} is equal to zero. By doing so we put ourselves in a Fickian-like framework, where the diffusive motion of each species depends only on the spatial profile of its own chemical potential and the chemical potential of the reference species (in this case, the empty sites). By additionally considering that the fluxes must recover the usual Fick equation for a binary mixture:

$$\lim_{c_Y(\mathbf{r},t)\to 0} \Phi_X = -D_X \nabla c_X(\mathbf{r},t), \qquad \lim_{c_X(\mathbf{r},t)\to 0} \Phi_Y = -D_Y \nabla c_Y(\mathbf{r},t), \tag{20}$$

one infers that the Onsager coefficients are given by

$$L_{XX} = \frac{D_X\, c_X(\mathbf{r},t)\, c*(\mathbf{r},t)}{c_t\, k_B}, \quad L_{YY} = \frac{D_Y\, c_Y(\mathbf{r},t)\, c*(\mathbf{r},t)}{c_t\, k_B},$$

which closes the above expressions for the diffusion fluxes:

$$\Phi_X = D_X\left[\left(1 - \frac{c_Y}{c_t}\right)\nabla c_X + \frac{c_X}{c_t}\nabla c_Y\right], \tag{21}$$

$$\Phi_Y = D_Y\left[\frac{c_Y}{c_t}\nabla c_X + \left(1 - \frac{c_X}{c_t}\right)\nabla c_Y\right], \tag{22}$$

where we no longer write the spatiotemporal dependences, for the sake of a lighter notation.

Notice the presence of cross-diffusive terms in the right-hand side of Eqs. (21) and (22). Because of the balance (7), the effective chemical potential for the X species $[\mu_X - \mu_*]$ depends on the concentration of Y, and vice versa for Y. This simple source of nonideality naturally produces the above cross-diffusive terms even though we ruled out the thermodynamic cross couplings between the diffusion fluxes and forces. It is noteworthy that the same expressions have also been derived from a mesoscopic, stochastic level of description and were shown to correspond to a random walk involving impenetrable particles [17,18].

C. Evolution equations

Based on all the above considerations, the reaction-diffusion equations for the lattice Brusselator model read

$$\frac{\partial c_X}{\partial t} = k_1\, a_A\, c_* - [k_2\, a_B + k_4]\, c_X + k_3\, c_X^2\, c_Y + D_X\left[\left(1 - \frac{c_Y}{c_t}\right)\nabla^2 c_X + \frac{c_X}{c_t}\nabla^2 c_Y\right], \tag{23}$$

$$\frac{\partial c_Y}{\partial t} = k_2\, a_B\, c_X - k_3\, c_X^2\, c_Y + D_Y\left[\frac{c_Y}{c_t}\nabla^2 c_X + \left(1 - \frac{c_X}{c_t}\right)\nabla^2 c_Y\right]. \tag{24}$$

For analysis purposes, we introduce the rescaled quantities

$$\tau = t k_4, \quad x = c_X\sqrt{\frac{k_3}{k_4}}, \quad y = c_Y\sqrt{\frac{k_3}{k_4}},$$
$$a = a_A\frac{k_1}{k_4}c_t\sqrt{\frac{k_3}{k_4}}, \quad b = a_B\frac{k_2}{k_4}, \quad c = \frac{1}{c_t}\sqrt{\frac{k_4}{k_3}}, \tag{25}$$
$$\delta = \frac{D_X}{D_Y}, \quad \tilde{\nabla}^2 = \frac{D_Y}{k_4}\nabla^2.$$

Equations (23) and (24) then take the dimensionless forms

$$\frac{\partial x}{\partial \tau} = a - (b+1)\,x + x^2\,y - ac\,(x+y) + \delta[\tilde{\nabla}^2 x + c(x\tilde{\nabla}^2 y - y\tilde{\nabla}^2 x)], \tag{26}$$

$$\frac{\partial y}{\partial \tau} = bx - x^2 y + [\tilde{\nabla}^2 y + c(y\tilde{\nabla}^2 x - x\tilde{\nabla}^2 y)]. \tag{27}$$

Note that the values of the concentration variables in Eqs. (23) and (24) are restricted to the interval $[0,c_t]$, because of the balance (7). For the same reason, the maximum value allowed to the adimensional variables x and y is $1/c$. As a result, the parameter c can be seen as the one controlling the level of *molecular crowding*. Small values of c correspond to systems where the local concentration of nodes is large or, in other words, where a large number of molecules can be placed in each mesoscopic box. The ideal case of an infinitely diluted system is then found by letting $c \to 0$. In this limit, Eqs. (26) and (27) become identical to the evolution equations of the Brusselator model, which in this view represent the ideal limit of the lattice Brusselator. Inversely, larger values of c correspond to more restricted environments, where nonideal effects are expected to come into play.

Let us turn now to the analysis of the above equations, for both the homogeneous and the spatially distributed cases.

III. DYNAMICS IN A WELL-STIRRED SYSTEM

Consider the case where the system is perfectly mixed, so that no gradient of composition can develop. Equations (26) and (27) become

$$\frac{dx}{dt} = a - (b+1)\,x + x^2 y - ac\,(x+y), \tag{28}$$

$$\frac{dy}{dt} = bx - x^2 y\ . \tag{29}$$

This system of equations can present up to three steady-state solutions, given by

$$\overline{x}_1 = 0, \quad \overline{y}_1 = \frac{1}{c}, \tag{30}$$

$$\overline{x}_2 = \frac{a + \sqrt{a(a-4bc-4abc^2)}}{2+2ac}, \qquad \overline{y}_2 = \frac{a - \sqrt{a(a-4bc-4abc^2)}}{2ac}, \tag{31}$$

$$\overline{x}_3 = \frac{a - \sqrt{a(a-4bc-4abc^2)}}{2+2ac}, \qquad \overline{y}_3 = \frac{a + \sqrt{a(a-4bc-4abc^2)}}{2ac}. \tag{32}$$

The simplicity of the model allows one not only to extract exact expressions for these steady states, but also to analytically test their stability and check for the presence of bifurcations.

The first solution (state 1) always exists and corresponds to a system without X particles, and totally covered in Y, so that none of the elementary reactions can take place: We will therefore often refer to it as the poisoned state, or simply the poisoning, borrowing from the usual terminology of surface reactions. A linear stability analysis performed around this state shows that it is always a *stable node*. The other fixed points (2 and 3), which we will refer to as the reactive states, exist only when the polynomial under the square root in (31) and (32) is positive, or equivalently whenever

$$b < b_{LP} \quad \text{with} \quad b_{LP} = \frac{a}{4c + 4ac^2}. \tag{33}$$

When $b = b_{LP}$ these two fixed points collide and annihilate each other, i.e., the system undergoes a *limit point bifurcation*. Linear stability analysis shows that state 3 is always a *saddle*, while state 2 can be either a *node* or a *spiral*, as the real parts of the two eigenvalues of the corresponding linearized matrix have the same sign. State 2 can undergo a *Hopf bifurcation* whenever this real part crosses zero, which happens for a critical value of $b = b_H$:

$$b_H = \frac{2 + a^2 + 8ac + 10a^2c^2 + 4a^3c^3 + \sqrt{a^4 - 4a^3c - 12a^4c^2 - 8a^5c^3}}{2(1 + 4ac + 4a^2c^2)} \tag{34}$$

with the additional conditions $c \leqslant \sqrt{3}/9$ and $a_{H_{\min}} < a < a_{H_{\max}}$, where $a_{H_{\min}}$ and $a_{H_{\max}}$ are the real positive solutions of

$$4a^3c^4 + 12a^2c^3 + a(12c^2 - 1) + 4c = 0. \tag{35}$$

State 2 becomes unstable in the range $b_H \leqslant b \leqslant b_{LP}$: These conditions thus delimit a volume in parameter space where oscillations of the concentrations should be expected.

Numerical integrations of the fully nonlinear system confirm the validity of the above picture, as shown for example in the bifurcation diagram of Fig. 1, where b was chosen as the control parameter. For small b, one encounters a region of bistability between states 1 and 2, where state 3 defines the separatrix. As expected, sustained oscillations, described by a limit cycle in the phase space, are observed as soon as one crosses b_H. The system is then characterized by the coexistence of an oscillatory reactive state and a steady poisoned state, again separated by state 3 (see Fig. 2 for some examples of time-dependent trajectories). Note in Fig. 1 that the amplitude of the oscillations increases with b, until it is large enough that the limit cycle intercepts the saddle point, forming a homoclinic orbit for a critical value of $b = b_{HC}$. A *homoclinic bifurcation* thus destroys the oscillatory regime and, for further increases in b, the only global attractor of the system is the poisoned state 1. Nevertheless, the trajectories in the phase space can still "feel" the presence of the two other states, in the sense that state 1 presents a region of excitability that extends even beyond the limit point bifurcation, to a close neighborhood of $b > b_{LP}$.

A convenient way to visualize how the states and bifurcations emerge is to see how the different regions in the $\{a,b\}$ plane change, for increasing values of c (see Fig. 3). For $c = 0$ [Fig. 3(a)], only the reactive steady state 2 exists, which can be either stable (uncolored region I) or unstable (dark gray area II): In this latter case, sustained oscillations are observed. As soon as $c > 0$ [Fig. 3(b)], states 1 and 3 appear and region I now corresponds to a bistability between states 1 and 2. Similarly, in region II, one finds the above-mentioned coexistence of oscillations and poisoning, separated by a saddle. This region is however now sandwiched between the Hopf bifurcation line and a curve corresponding to the homoclinic bifurcation [the dotted line in Fig. 3(b)]. One also observes the emergence of two new dynamical regions, denoted III and IV. Region III corresponds to situations where a stable state 1 coexists with unstable states 2 and 3, but oscillations are not present. In region IV the only existing steady state is the poisoning. As c continues to increase, the poisoned region expands while the oscillatory domain shrinks [see Fig. 3(c)]. Eventually c reaches its limiting value $c = \sqrt{3}/9$ and the domain where the steady state 2 is unstable vanishes [Fig. 3(d)]. Further increasing c extends the poisoned domain with respect to the reactive one.

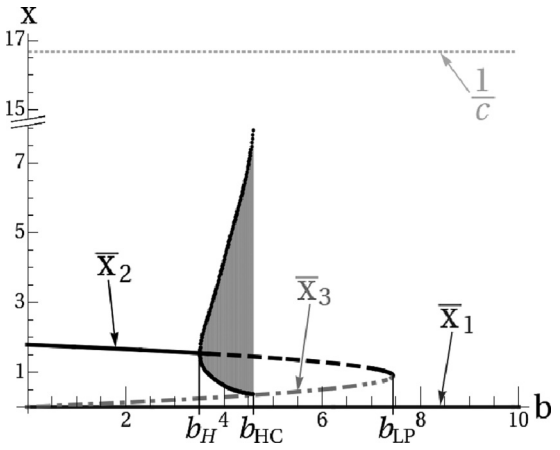

FIG. 1. Bifurcation diagram, showing the asymptotic values of x obtained when using b as a control parameter. The stability of the three states is given by the line style: continuous line for stable states, dashed line for unstable states, and dash-dotted line for saddle points. In the regions where sustained oscillations are found, we plot the minimal and maximal values of x. The other parameters of the model take the following values: $a = 2$, $c = 0.06$. The line on top indicates the maximal possible value for x.

A. Effect of nonideality

It is relevant at this stage to turn back to the original Brusselator, to better understand the role played by spatial restrictions in the dynamical complexity of the lattice Brusselator. The Brusselator was derived by considering that the reactive system is ideal, i.e., by assuming that molecules are interactionless, pointlike particles placed in an infinite medium. It is characterized by a single homogeneous steady state given by $\overline{x}_{\rm Br} = a$ and $\overline{y}_{\rm Br} = b/a$, which can only undergo a Hopf bifurcation, taking place at $b_H^{\rm Br} = a^2 + 1$. This picture is qualitatively very different from the dynamical characteristics we just presented. Simply including a concentration cap is enough to multiply the complexity of the chemical kinetics: This restriction adds two more steady states and two new bifurcations to the scheme. The two systems (the original and the lattice Brusselators) should however converge in the limit

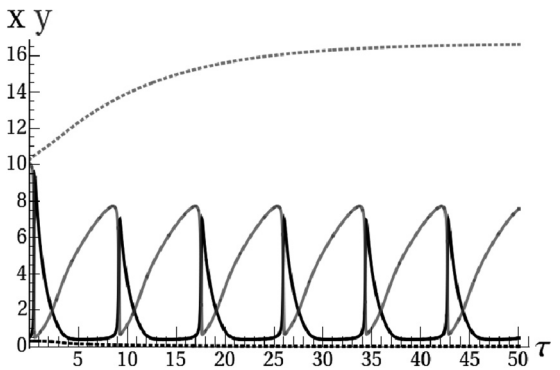

FIG. 2. Time evolution of x (black) and y (gray) for two close initial conditions centered around the separatrix, respectively at $\{x,y\} = \{0.48, 10.07\}$ (continuous lines) and $\{x,y\} = \{0.30, 10.27\}$ (dashed lines). One can observe a bistability between poisoning and oscillations, as mentioned in the text. The control parameters are $a = 2$, $b = 4.5$, and $c = 0.06$.

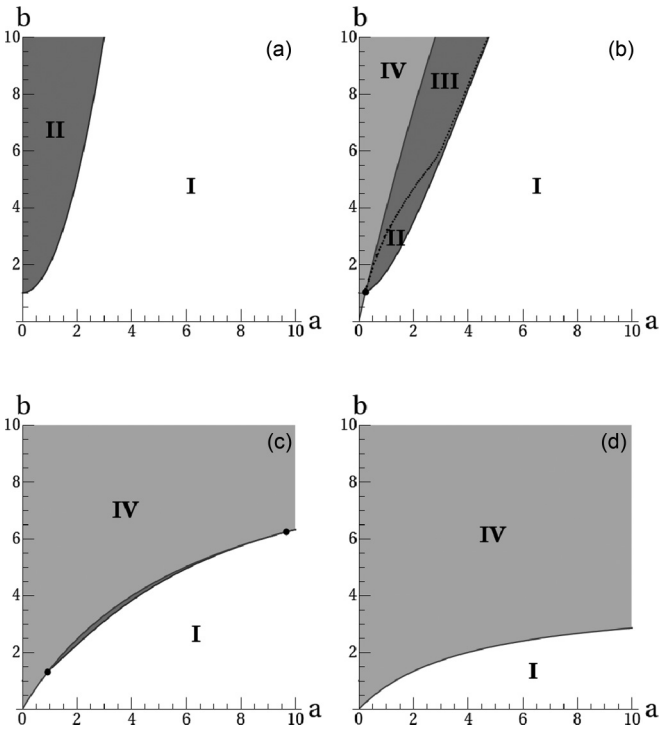

FIG. 3. Dynamical regions and bifurcation lines in the $\{a,b\}$ plane for four values of c: (a) $c = 0$; (b) $c = 0.06$; (c) $c = 0.155$; (d) $c = 0.25$. The steady state 2 is stable in the white region, and becomes unstable in the dark gray region between the two big black dots with respective abscissas $a_{H_{\rm min}}$ and $a_{H_{\rm max}}$. The gray and black lines separating the different regions are the analytical expressions for $b_{\rm LP}$ and b_H, while the dots in (c) are the numerical estimate of the homoclinic bifurcation points. Note that in (c) the homoclinic bifurcation becomes extremely close to the Hopf one, and for any practical purpose one does not observe a limit cycle anymore.

where this spatial constraint is relaxed, in other words when $c_t \to \infty$ or, equivalently, $c \to 0$. We shall thus investigate this limit in more detail.

The three fixed points of the lattice Brusselator greatly differ in their behavior as $c \to 0$. From the analytical expressions (31) one gets for state 2

$$\lim_{c\to 0} \overline{x}_2 = a, \quad \lim_{c\to 0} \overline{y}_2 = \frac{b}{a},$$

which is nothing else than the only fixed point of the original Brusselator. This state can only undergo a Hopf bifurcation, since $\lim_{c\to 0} b_{\rm SN} = \infty$ while $\lim_{c\to 0} b_H = a^2 + 1$ (and the other constraints are automatically respected). This reactive state can thus be seen as a "smooth" prolongation of the ideal behavior in a restricted environment, the influence of which can in consequence be estimated through, say, a development in series using c as a small parameter. For example, one can estimate that for small values of c,

$$\overline{x}_2 = a - (a^2 + b)c + O(c^2), \tag{36}$$

$$\overline{y}_2 = \frac{b}{a} + \frac{b(a^2 + b)}{a^2}\, c + O(c^2), \tag{37}$$

$$b_H = a^2 + 1 - (4a^3 + a)c + O(c^2). \tag{38}$$

This development sheds some light on the role of spatial constraints on the steady states. Indeed, it appears that finite size effects tend to decrease the amount of X particles and increase the quantity of Y. Qualitatively speaking, the main reason for this resides in the way these species are injected in the system. In the original Brusselator, the inflow of X is constant and solely determined by the parameter a. The spatial constraints included in the lattice Brusselator result in a modified inflow term, which now is directly proportional to the amount of available free space. In comparison with the ideal case, including the effect of molecular crowding (increasing c) will result in a lower flux of X for any given value of a, which will in turn induce a lower steady-state concentration for that species. Since the fixed point always respects $\overline{x}_2\,\overline{y}_2 = b = \text{const}$, the concentration in Y consequently increases.

Since state 2 corresponds to the only fixed point of the original Brusselator, one might wonder what happens to the two other steady states in the limit of ideal systems. The analytical expressions (30) and (32) show that states 1 and 3 actually merge in this limit:

$$\lim_{c\to 0}\overline{x}_1 = \lim_{c\to 0}\overline{x}_3 = 0,$$

$$\lim_{c\to 0}\overline{y}_1 = \lim_{c\to 0}\overline{y}_3 = \lim_{c\to 0}\frac{1}{c} = \infty.$$

This "merged state" formally corresponds to a poisoning of the system by species Y but its concentration now tends to infinity, which explains why it cannot be observed in the ideal limit. In other words the original Brusselator can be seen as a limit model, which captures the local dynamics around only one of the existing states, in a region of phase space where $c_X + c_Y \ll c_t$.

IV. DYNAMICS IN THE SPATIALLY DISTRIBUTED SYSTEM

In this section we will explore the qualitative behavior of the lattice Brusselator in spatially distributed systems, to see how crowding may affect pattern formation. A detailed study and classification of all the different dynamical scenarios is beyond the scope of the present paper. We will herein focus on how the molecular crowding affects the formation of stationary patterns.

Let us define the *base states* of the lattice Brusselator as the spatially homogeneous stationary solutions of Eqs. (26) and (27), i.e., the states defined by (30)–(32). A spatial pattern of concentrations may arise whenever one of these states loses its stability with respect to small periodic spatiotemporal perturbations of wave number κ. It can be shown that state 1 is in this view always stable. This is reasonable and could be expected also on the grounds of simple physical insight: Since Y saturates the whole space and the concentration of X is null, a periodic modulation around this state would imply the existence of regions with a negative value of c_X where c_Y would exceed the maximum allowed value.

State 2 can be destabilized via a Turing bifurcation, as one of its corresponding real eigenvalues can cross zero for nonzero values of the wave number κ. An exact analytical expression of the bifurcation point could be found by linear stability analysis but is too cumbersome to be of any help in interpreting the role of the spatial constraints. However, by expanding the base state 2 in series of c [see Eqs. (36) and (37)] and then performing linear stability analysis around this state, one can verify that the lattice Brusselator shows a *Turing instability* with characteristic wave number κ_T for values of $b \geqslant b_T$, with

$$b_T = (1+\delta^{1/2}a)^2 - 2[(1+\delta^{1/2}a) \times \{2\delta^{1/2} + a[-1 + a\delta + 2a\delta^{3/2})]\}c + O(c^2), \quad (39)$$

$$\kappa_T^2 = \frac{a}{\delta^{1/2}} - \frac{(1+\delta^{1/2}a)^2}{\delta^{1/2}}c + O(c^2) \quad (40)$$

Remember that the original Brusselator can also undergo such an instability, for $b \geqslant b_T^{\mathrm{Br}} = (1+\delta^{1/2}a)^2$ and with $\kappa_T^{\mathrm{Br}2} = a\delta^{-1/2}$. Since the instability condition for the lattice Brusselator emerges in a continuous way from this value, one can use expression (39) to build some insight into the role of confinement in the development of patterns with respect to the reference ideal case.

First, it should be noted that the spatial constraints displace the Turing bifurcation point. The relative location of b_T with respect to b_T^{Br} depends on the sign of the linear term in c in the right-hand side of Eq. (39). It can thus in principle be larger or smaller than its value in the ideal limit. Ultimately the problem translates into studying the sign of the polynomial

$$-a^2\delta(1+\delta^{1/2}) + a - 2\delta^{1/2}, \quad (41)$$

which becomes positive (i.e., postpones the instability) for

$$\frac{1}{2\delta(1+\delta^{1/2})}[1-\sqrt{1-8(\delta^{3/2}+\delta^2)}] < a < \frac{1}{2\delta(1+\delta^{1/2})}[1+\sqrt{1-8(\delta^{3/2}+\delta^2)}]. \quad (42)$$

From the Brusselator analysis, we know that a necessary condition to observe stationary patterns is that the autocatalytic species X must diffuse less rapidly than Y or, in mathematical terms, $\delta < 1$. In a recent study, Fanelli *et al.* [19] show that this requirement is not needed in lattice systems with cross-diffusive terms in general, and for the lattice Brusselator in particular. The authors could trace back this surprising conclusion to a competition of the active species for empty sites: This kind of behavior is to be expected for highly crowded systems (as in the example reported by Fanelli *et al.*), which is far beyond the linear regime defined by Eqs. (39) and (40) and thus cannot be predicted using the proposed development. Within the range of validity of the above equations, however, and for $\delta \ll 1$ it can easily be checked that the linear term in c in (39) is always positive. As a consequence the value of b_T increases with c when this parameter is not too large, until the Turing bifurcation ultimately approaches, and collides with, the Hopf bifurcation point b_H. The spatial restrictions thus generically tend to narrow the region of the parameter space where Turing patterns are expected to be observed. This is confirmed by numerical integration of the fully nonlinear problem, which also shows that the trend remains qualitatively the same for relatively large values of $\delta < 1$.

Crowding affects not only the location of the Turing bifurcation point, but also the amplitude and (to a lesser extent)

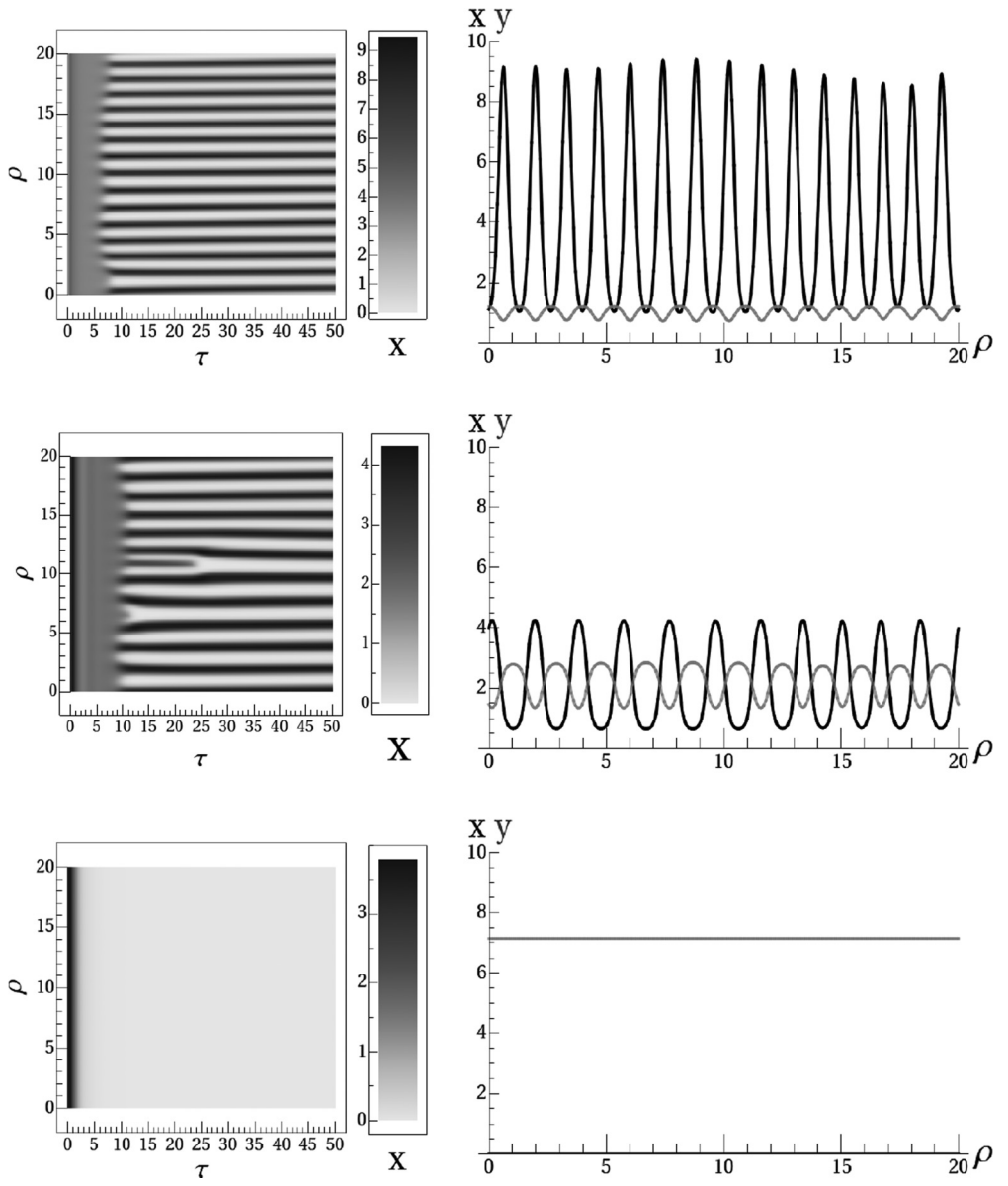

FIG. 4. Space-time plots for x (left side) and long-term spatial profiles (right side) for x (black line) and y (gray line) for the one-dimensional lattice Brusselator. ρ is the spatial coordinate indirectly defined by the nondimensional Laplacian $\tilde{\nabla}^2$ in (25). All the plots come from numerical integrations of the lattice Brusselator's reaction-diffusion equations performed with $a = 4$, $b = 5$, $\delta = 0.05$, with c taking values of 0 (top), 0.1 (middle), and 0.14 (bottom). The total simulation time is $\tau = 50$ and the spatial domain has periodic boundary conditions. The spatial profiles on the right column are taken at $\tau = 50$.

the shape of the patterns that are formed. On the contrary, it apparently does not impact as much the wavelength of the instability, which can also be deduced from the expression (40) for κ_T in the typical range of parameter values where Turing patterns appear (i.e., $\delta, c \ll 1, a$). Figure 4 illustrates how increasing values of c affect the amplitude of the Turing pattern, for fixed values of the other parameters. Typically, both the average value and the amplitude of oscillations of x decrease, while the same quantities slightly increase for y. This trend is consistent with the displacement of the steady states that we commented on in the previous section. Higher levels of crowding correspond to slower inflows of X from the external reservoir and hence to lower concentrations of this species inside the restricted environment. The amount of Y particles adjusts itself due to the balance between the different elementary steps. Above a certain value of c, the oscillatory pattern is no longer observed and the system shows only a uniform steady state corresponding to the poisoning. In the examples we show here, the disappearance of the Turing pattern can be imputed to the crossing of the above-mentioned limit point bifurcation. Generally speaking though, a "death" of patterns may be observed even before the system passes through this bifurcation. Indeed, the Turing bifurcation takes place in a region of the parameter space where a bistability is found between the reactive and poisoned states. The long-term dynamics of the system thus depends not only on the choice of parameters, but also on the chosen initial conditions (as shown in Fig. 5).

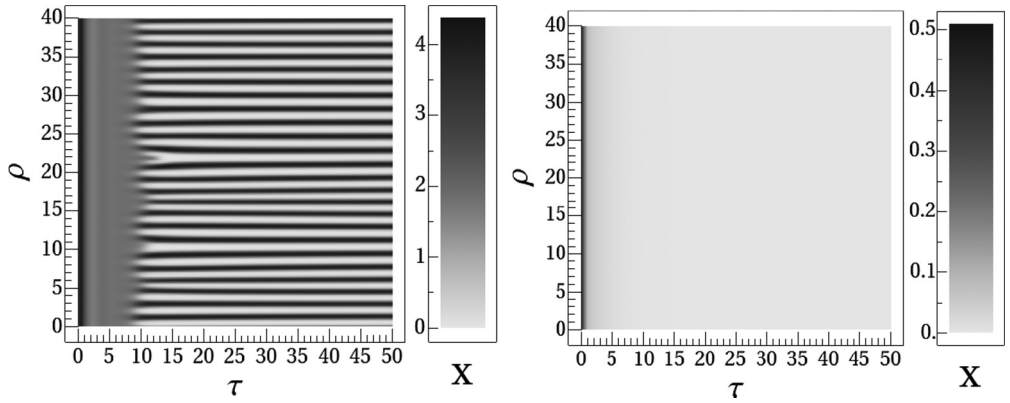

FIG. 5. Space-time plots of x for two different initial conditions of the one-dimensional lattice Brusselator. The plots come from numerical integrations performed with $a = 4$, $b = 5$, $\delta = 0.05$, and $c = 0.1$. The total simulation time and boundary conditions are the same as in Fig. 4. The initial conditions for the left and right plots are respectively $\{x,y\} = \{3.5,3.5\}$ and $\{x,y\} = \{0.5,8.5\}$.

The whole dynamical picture of the spatially extended case is quite complex. In addition to the aforementioned coexistence of poisoned and periodic patterns, the presence of the Hopf bifurcation is also expected to play an important role. As mentioned earlier, though, our goal here was not to study extensively all the possible scenarios, but rather to highlight how spatial constraints affect the structure of the original Brusselator's bifurcation diagram. We will thus now summarize our main findings and discuss the consequences and potential extensions of our study.

V. CONCLUSIONS

Numerous studies of chemical oscillators, mostly based on microscopic or mesoscopic simulations, showed behaviors that differ substantially from the predictions of the traditional reaction-diffusion approach. In this work, our goals were (i) to assess whether these equations should not be themselves modified because of the geometrical constraints and (ii) if so, to what extent these modifications can affect oscillatory schemes. We thus developed and studied a lattice gas version of the Brusselator model, the lattice Brusselator, as a prototype to investigate the effect of molecular crowding on oscillating reactions.

We used nonequilibrium thermodynamics to derive the modified reaction-diffusion equations that incorporate such geometrical constraints. Both the reaction and the diffusion terms turned out to be affected. By analyzing these amended evolution laws, we could highlight two main trends:

(1) The spatial constraints modify the value of the original, ideal steady states and displace the bifurcations these states can undergo.

(2) Qualitatively different solutions (which might be be steady or time and/or space dependent) emerge whenever such constraints are taken into account. These solutions can interact with the already existing ones, leading to a globally more complex dynamical picture.

In each of these cases, molecular crowding proved to play a pivotal role. It is noteworthy that this occupancy effect can be quantified and tuned at will through a single adimensional parameter c, which is proportional to the inverse of the maximal attainable concentration. We expect the above trends to hold true for different sorts of reactive systems in restricted environments, such as biological cells, low-dimensional substrates, or micro- or nanostructured materials.

The very emergence of additional states in constrained environments is not completely unexpected. This was already noted in models of heterogeneous catalysis [20], in which the competition for empty surface sites plays the role of an additional feedback acting on the dynamical variables. This seems to be a general trend whenever hard-core repulsion is incorporated. Similarly, the coexistence of oscillatory and steady states had already been observed in models of surface reactions [21]. Our study thus confirms that nonlinear reactions taking place in restricted environments tend to generate multistability. This fact was however not referred to in the simulation-based studies in which "new states" were observed [11]. It would be interesting to analyze these models again to understand which phenomena are due to nonideality, and what can actually be linked with the emergence of strong spatial correlations.

On the contrary, the role played by the restricted geometry in transport has been disregarded in many circumstances thus far. Nonideal reaction rates have typically been combined with ideal diffusion terms. Such an asymmetric combination is not expected to correctly describe the spatiotemporal behavior of crowded systems, since Fickian diffusion does not respect the conservation laws imposed by the medium constraints. Some recent investigations [8,22], including this work, show that transport can be strongly affected by crowding effects as well. It would thus be interesting to analyze how the conclusions drawn in the limit of ideal diffusion are affected by nonideal contributions.

The present investigations open the way to several future works. First of all, the lattice Brusselator, although relatively simple, presents a variety of dynamical phenomena that can be analyzed in details thanks to the simplicity of the model. This could include for example Turing-Hopf interactions, stability analyses of coexisting periodic and flat concentration patterns, excitable waves, and so on. Another future extension concerns the case of systems with short-ranged repulsive interactions (as in this paper) coupled to attractive ones. Attractive interactions are known to induce phase transitions at equilibrium as well as far from it. A thermodynamically consistent treatment of

the effects of such nonidealities on autocatalytic schemes has already been brought to light some time ago by Carati and Lefever [23]. As we just saw, though, hard-core repulsions on a lattice are enough to induce bistability by themselves. The combination of these two effects could lead to unexpectedly complex behaviors, even in the case of rather simple reactions, and we believe that clarifying this situation is certainly worth investigating.

It should also be noticed that, although the present study clarifies the nonequilibrium thermodynamic status of the lattice Brusselator, we can already individuate at least two situations for which some of the hypotheses we used here might not be valid. First, in highly crowded systems the reduced mobility of the particles may not allow a time scale separation between transport and reactive events, which endangers the validity of the local equilibrium hypothesis. Second, it is now well known that the mean field hypothesis can break down in the case of low-dimensional reactive systems. The local fluctuations of composition due to the stochastic character of the elementary events are not washed out easily in such systems, because of the poor efficiency of mixing through diffusion on low-dimensional supports. Short-ranged, large correlations can thus build up and affect the overall dynamics. This discrepancy is particularly strong in the case of highly nonlinear elementary steps taking place on networks of low coordination (e.g., termolecular steps on low-dimensional regular lattices [24]). We are thus investigating right now, for the lattice Brusselator, the differences between mesoscopic simulations and the above mean field treatment. These results will be presented soon in a work aimed at clarifying the relative importance of the fluctuations and the mean-field-type terms that we present here, with a special emphasis being put on the connection between the microscopic details of the reactive mechanism and the range of validity of the mean field prediction.

ACKNOWLEDGMENT

The present work was partially supported by the FUNC-DYN research networking program of the European Science Foundation.

APPENDIX: DERIVATION OF THE THERMODYNAMICAL FORCES FOR MASS TRANSPORT

Our starting point is the entropy production $\sigma_{\rm diff}$ due to the diffusive motion given by classical nonequilibrium thermodynamics [14]. In the absence of temperature gradients one formally has in the problem being studied

$$T\sigma_{\rm diff} = -\left[\frac{\mathbf{j}_X}{M_X}\cdot\nabla_T\mu_X + \frac{\mathbf{j}_Y}{M_Y}\cdot\nabla_T\mu_Y + \frac{\mathbf{j}_*}{M_*}\cdot\nabla_T\mu_*\right], \tag{A1}$$

where M_i and $\mathbf{j}_i$ are the molar masses and the *mass diffusive fluxes* of the ith species, the latter being defined as the displacement flux with respect to the center of mass velocity $\mathbf{v}$:

$$\frac{\mathbf{j}_i}{M_i} = \Phi_i - c_i\mathbf{v} \qquad \text{for} \quad i = X, Y, *\,. \tag{A2}$$

Our aim is to rewrite (A1) in terms of the natural transport fluxes of our system Φ_X and Φ_Y, in order to find the correct form of the associated thermodynamic forces and then carry on the linear expansion (18) and (19). Notice that although the *mole averaged velocity* $\mathbf{u} = \frac{\Phi_X+\Phi_Y+\Phi_*}{c_t}$ is null by virtue of (17), nothing can be said in principle about $\mathbf{v}$; furthermore the diffusive balance $\mathbf{j}_X + \mathbf{j}_Y + \mathbf{j}_* = 0$ does not apply to the quantities $\frac{\mathbf{j}_i}{M_i}$ if the molar masses of the three species are different. Therefore in principle we should not be able to substitute the molar fluxes for the mass diffusive ones.

However, this limitation can here be overcome because, in a lattice gas formulation, the species behave as perfect gases, and because we also assumed that the total concentration c_t and the temperature T are constant in both time and space. The gradient of pressure becomes at each point thus is given by

$$\nabla p = \nabla(k_B T c_t) = 0. \tag{A3}$$

Since there is no external force field acting on the system, Eq. (A3) coincides with the *mechanical equilibrium* condition. We can therefore invoke a theorem proved by Prigogine [25] according to which, in order to calculate the entropy production, the barycentric velocity $\mathbf{v}$ can be replaced with any other reference velocity. By replacing $\mathbf{v}$ with $\mathbf{u}$, the entropy production by diffusion becomes

$$\sigma^{\rm diff} = -\Phi_X\cdot\frac{\nabla_{T,p}(\mu_X-\mu_*)}{T} - \Phi_Y\cdot\frac{\nabla_{T,p}(\mu_X-\mu_*)}{T}. \tag{A4}$$

Equation (A4) is now expressed in terms of the molar fluxes Φ_X and Φ_X, to which correspond the thermodynamic forces $\frac{\nabla_{T,p}(\mu_X-\mu_*)}{T}$ and $\frac{\nabla_{T,p}(\mu_X-\mu_*)}{T}$.

[1] G. Nicolis and I. Prigogine, *Self Organization in Nonequilibrium Systems* (Wiley, New York, 1977).
[2] B. Temel, H. Meskine, K. Reuter, M. Scheffler, and H. Metiu, J. Chem. Phys. **126**, 204711 (2007).
[3] G. Odor, Rev. Mod. Phys. **76**, 663 (2004).
[4] A. P. Minton, J. Biol. Chem. **276**, 10577 (2001).
[5] K. Takahashi, S. N. Arjunan, and M. Tomita, FEBS Lett. **579**, 1783 (2005).
[6] R. Grima and S. Schnell, Biophys. Chem. **124**, 1 (2006).
[7] S. Prakash and G. Nicolis, J. Stat. Phys. **86**, 1289 (1997).
[8] Y. De Decker and F. Baras, Eur. Phys. J. B **78**, 173 (2010).
[9] A. Provata, G. Nicolis, and F. Baras, J. Chem. Phys. **110**, 8361 (1999).
[10] A. V. Shabunin, F. Baras, and A. Provata, Phys. Rev. E **66**, 036219 (2002).
[11] V. P. Zhdanov, Phys. Chem. Chem. Phys. **3**, 1432 (2001).

[12] T. Rao, Z. Zhang, Z. Hou, and H. Xin, Chin. J. Chem. Phys. **24**, 425 (2011).
[13] I. Prigogine and R. Lefever, J. Chem. Phys. **48**, 1695 (1968).
[14] S. R. De Groot and P. Mazur, *Non-Equilibrium Thermodynamics* (North Holland, Amsterdam, 1969).
[15] T. L. Hill, *An Introduction to Statistical Thermodynamics* (Courier Dover Publications, New York, 1960).
[16] I. Prigogine, *Introduction to Thermodynamics of Irreversible Processes* (Interscience, New York, 1955).
[17] D. Fanelli and A. J. McKane, Phys. Rev. E **82**, 021113 (2010).
[18] M. Asslani, F. Di Patti and D. Fanelli, Phys. Rev. E **86**, 046105 (2012).
[19] D. Fanelli, C. Cianci, and F. Di Patti, Eur. Phys. J. B **86**, 142 (2013).
[20] M. Feinberg and D. Terman, Arch. Ration. Mech. Anal. **116**, 35 (1991).
[21] R.-S. Li and W. Horsthemke, J. Chem. Phys. **95**, 5785 (1991).
[22] D.-J. Liu and J. W. Evans, J. Chem. Phys. **125**, 054709 (2006).
[23] D. Carati and R. Lefever, Phys. Rev. E **56**, 3127 (1997).
[24] A. Tretyakov, A. Provata, and G. Nicolis, J. Chem. Phys. **99**, 2770 (1995).
[25] I. Prigogine, *Etude Thermodynamique des Phénomènes Irréversibles* (Desoer, Liège, 1947).